Applied Catalysis B: Environmental 193 (2016) 189–197

Contents lists available at ScienceDirect

Applied Catalysis B: Environmental

journal homepage: www.elsevier.com/locate/apcatb

New insights into the primary roles of diatomite in the enhanced sequestration of UO_2^{2+} by zerovalent iron nanoparticles: An advanced approach utilizing XPS and EXAFS

Guodong Sheng[a,b,*], Pengjie Yang[a], Yanna Tang[a], Qingyuan Hu[a], Hui Li[a], Xuemei Ren[d], Baowei Hu[a,*], Xiangke Wang[a,b], Yuying Huang[c]

[a] College of Chemistry and Chemical Engineering, College of Yuanpei or College of Medical Science, Shaoxing University, Zhejiang 312000, PR China
[b] School of Chemistry and Environment, North China Electric Power University, Beijing 102206, PR China
[c] Shanghai Synchrotron Radiation Facility (SSRF), Shanghai Institute of Applied Physics, Chinese Academy of Sciences, Shanghai 201204, PR China
[d] Institute of Plasma Physics, Chinese Academy of Sciences, P.O. Box 1126, Hefei 230031, PR China

ARTICLE INFO

Article history:
Received 5 January 2016
Received in revised form 3 April 2016
Accepted 16 April 2016
Available online 19 April 2016

Keywords:
Diatomite
Nanoscale zero valent iron
Enhanced U(VI) sequestration
Primary roles

ABSTRACT

In the current paper, nanoscale zero-valent iron (NZVI) was immobilized onto the negatively-charged diatomite to obtain a novel composite (NZVI-D) for the enhanced sequestration of uranyl (U(VI)) in water. The as-synthesized NZVI-D was characterized by SEM, TEM and XRD in detail, and better dispersion of NZVI on diatomite surface was observed, as compared with bare NZVI. The efficiency of U(VI) sequestration by NZVI-D was compared with that of commercial iron and bare NZVI. It was found that NZVI-D exhibits the best efficiency in U(VI) sequestration, showing obvious synergistic effect between diatomite adsorption and NZVI reduction. The primary roles were further revealed by complementary macroscopic and spectroscopic studies. XPS results indicated that reduction of highly toxic and mobile UO_2^{2+} into less toxic and mobile UO_2 could be enhanced using diatomite-supported NZVI. EXAFS analysis demonstrated that diatomite could react as a scavenger for insoluble products like UO_2, and thus more reactive sites could be used for U(VI) reduction. Besides, diatomite play multiple roles on pH buffering and preventing NZVI from aggregating and as adsorbent of Fe(II) produced in-situ during reaction for further U(VI) reduction. This study opens a new avenue for the practical application of NZVI and NZVI-D in environmental remediation.

1. Introduction

A growing number of groundwater has been contaminated by uranium (U) as a result of mining activities or improper disposal of nuclear waste. Hence, it is important to develop an effective and feasible approach for the remediation of U-contaminated wastewater rapidly and completely [1–6]. In the natural water ambient environment, U is often in the main oxidation states of U(IV) and U(VI) [1–6]. Generally regarding, the reduction of U(VI) to insoluble U(IV) decreases the mobility of U through precipitation of sparingly soluble U(IV) minerals, and thus has been proposed as an important technique to remediate U-contaminated water [6–9].

Since the discovery of Cantrell et al. [9], zero-valent iron (Fe^0 or ZVI) has been utilized as a reactive material for the remediation of U(VI) (UO_2^{2+}) and related metal ions in contaminated wastewater due to its great reduction ability and low cost [9–15]. Subsequently, a large number of investigations have been conducted with respect to the reaction kinetics and interaction mechanisms of ZVI and U(VI) by combined macroscopic and microscopic techniques in the past two decades [14–21]. It has been generally proposed that the removal of soluble U(VI) by ZVI can be portioned in three reaction pathways, namely, (i) reductive precipitation of U(VI) to less soluble U(IV) by Fe^0 and Fe(II)-bearing corrosion products like green rust, which is the main mechanism, (ii) surface adsorption of U(VI) on iron corrosion products, and (iii) coprecipitation between UO_2^{2+} ion with iron corrosion products [14–21]. To improve the reduction performance, in the last decade, nanoscale zero-valent iron (NZVI) has been confirmed showing a better application prospect for the removal of U(VI) in water, which is due to the better inject ability into aquifer systems, higher reactive surface area, faster and more complete reactions [6–8,22–29]. However, there exist great limiting issues associated with the practical application

* Corresponding authors at: Shaoxing University, Zhejiang 312000, PR China
E-mail addresses: gdsheng@usx.edu.cn (G. Sheng), hbw@usx.edu.cn (B. Hu).

http://dx.doi.org/10.1016/j.apcatb.2016.04.035
0926-3373/

of NZVI currently, i.e., NZVI nanoparticle has a strong tendency to agglomerate into larger particles which leads to decrease its reactivity in application condition. Meanwhile, the aggregation of NZVI could also decrease its mobility in the subsurface, and thus a lot of researches have been done to modify the particles to improve this. Besides, the freshly-prepared NZVI can be easily oxidized and thus iron corrosion products can be formed on the surfaces, bringing the redox reaction to a halt [8,30–32]. Recently, this aggregation phenomenon have been reported to be considerably decreased when a support is used during the production of NZVI, and the synthesized NZVI in this way exhibits a narrower size distribution. Thus, the supported NZVI show much higher reactivity than bare NZVI does [33–53]. The synthesis of NZVI has been achieved in the presence of a large number of porous supports such as attapulgite [33], illite [34], montmorillonite [35], rectorite [36], bentonite [37,38], silica-based mesoporous or nanomaterials [39–42], resin [43,44], $Mg(OH)_2$ nanocrystals [45], and carbon-based materials [46–53]. All these papers indicated that the as-synthesized supported NZVI is a promising material in the environmental remediation of wastewater containing different kinds of metal ions. Nevertheless, the multi-roles of these supports in the NZVI reaction system have not been well revealed, particularly at a molecule level.

Diatomite with porous structure, which is a kind of natural amorphous siliceous mineral, possesses many unique properties including high porosity and permeability, excellent thermal and mechanical stabilities, chemical inertness. Thus, diatomite has been widely utilized as catalyst carriers, filter agents and wastewater treatment materials [54–58]. Besides, diatomite may be particularly suitable to be utilized as a support for NZVI due to its porous structure allowing high hydraulic conductivity, which should be in favor of conducting effluent to the reactive cites of the supported NZVI, resulting in faster removal rates in water system [59]. However, up to now, only a few studies on the removal performance of diatomite-supported NZVI have been reported [59,60]. Especially, to our knowledge, the primary roles of diatomite as a support in the NZVI treatment system have not been comprehensively investigated.

In the current paper, a novel composite namely diatomite-supported nanoscale zero-valent iron (NZVI-D) was synthesized and used to sequester uranyl ions (U(VI)) in water. The as-synthesized composite was characterized by X-ray diffraction (XRD), scanning electron microscope (SEM) and transmission electron microscope (TEM). Herein, the reductive transformation and sequestration performance of U(VI) into U(IV) by NZVI-D was investigated by batch experiments, and compared with that by bare NZVI. The reaction products were studied by using advanced approaches namely X-ray photoelectron spectroscopy (XPS) and X-ray absorption fine structure (XAFS). The primary roles of diatomite, including adsorbent of U(VI), pH buffering effect, scavenger for insoluble reaction products (UO_2), and finally adsorbent of Fe(II) for further reduction of U(VI), in U(VI) sequestration by NZVI were firstly revealed via complementary macroscopic and spectroscopic studies.

2. Experimental methods

2.1. Materials and chemicals

The chemicals like $UO_2(NO_3)_2{\cdot}6H_2O$, $FeSO_4{\cdot}7H_2O$, $NaBH_4$ and arsenazo(III) were purchased in analytical purity and used without further purification in our experiments. All solutions were prepared with 18 MΩ cm de-ionized water (Milli-Q Gradient, Millipore, and USA) under ambient condition. Commercial iron power (ZVI) was purchased from Shanghai Chemical, China, and the size passing through a sieve of 100 mesh (<150 μm) was used. The diatomite was obtained from Shengzhou County (Zhejiang, China). The raw samples were firstly physically purified in a centrifugal field in order to remove some impurities, then, the sample was processed by acid-leaching in 1.0 mol/L HCl solutions according to a previous paper [59]. The nanoscale zero valent iron (NZVI) was synthesized by a $NaBH_4$ reduction procedure according to the method which has been described in our previous work [8,53,61]. The diatomite-supported nanoscale zero valent iron (NZVI-D) were synthesized by a similar $NaBH_4$ reduction procedure for NZVI except that ~8.0 g of diatomite was soaking in $FeSO_4{\cdot}7H_2O$ solution under continuous stirring. These procedures are described in detail in the Supporting information (SI).

2.2. Experimental procedures

The sequestration of U(VI) by the reactive materials (i.e., diatomite, ZVI, NZVI and NZVI-D) was studied by using batch experiments which were carried out in a 100-mL conical flask at ~20 °C in water bath incubator under N_2 conditions. To collect enough solid products for spectroscopic analysis, the removal experiments of U(VI) were carried out in a 1000-mL conical flask, a certain amount of the reactive materials was mixed with 1000 mL of U(VI) solution with the concentration of 100 mg/L, After reaction for 120 min, the solid products were filtered through a 0.22 μm membrane, and then washed, finally vacuum-dried. The collected samples were stored in N_2 atmosphere. The reactive materials before and after reaction were characterized by X-ray diffraction (XRD), scanning electron microscope (SEM), transmission electron microscope (TEM), X-ray photoelectron spectroscopy (XPS), X-ray absorption fine structure (XAFS), N_2-BET and Zeta potentials. U L_3-edge XAFS spectra at 17166 eV for the reacted samples were recorded at room temperature at the beamline 14W in Shanghai Synchrotron Radiation Facility (SSRF, China). The detailed procedures for these microscopic experiments are shown in the SI.

3. Results and discussion

3.1. Preliminary characterization of the reactive materials

Preliminary characterization of the reactive materials using SEM, TEM, XRD and N_2-BET surface area suggested several physiochemical differences between these materials. The surface morphology of NZVI and NZVI-D was observed by SEM (Fig. 1A and B) and TEM images (Fig. S1A and B). We can see the as-synthesized NZVI dramatically assembles together and exhibits a chain-like structure, which is due to the magnetostatic attraction between iron particles. Nevertheless, for NZVI-D sample, it is evident that iron particles, elliptical in shape and with a size of ~100 nm, were randomly distributed and immobilized onto diatomite surfaces. This result indicates that diatomite as a support can weaken the aggregation effect of NZVI particles [59]. The XRD patterns of diatomite, NZVI and NZVI-D are shown in Fig. 1C. We can see that both NZVI and NZVI-D display a pure cubic α-Fe^0 crystalline structure with the main characteristic reflection at ~45.2° [59]. The previous studies suggested that NZVI might possess a typical "core–shell" structure including the existence of zero valent iron (core) and iron (hydr)oxides (shell) [59]. However, we can hardly find such observation in the XRD patterns herein, which might be caused from the low crystallinity of iron (hydr)oxides phases [59]. The broad reflection centered at ~21.5° in the XRD pattern of the diatomite sample is in good consistent with that of the referenced amorphous opal-A [59]. The presence of the broad reflection that is characteristic of diatomite in the NZVI-D sample indicated that low-crystalline iron species were well dispersed on diatomite

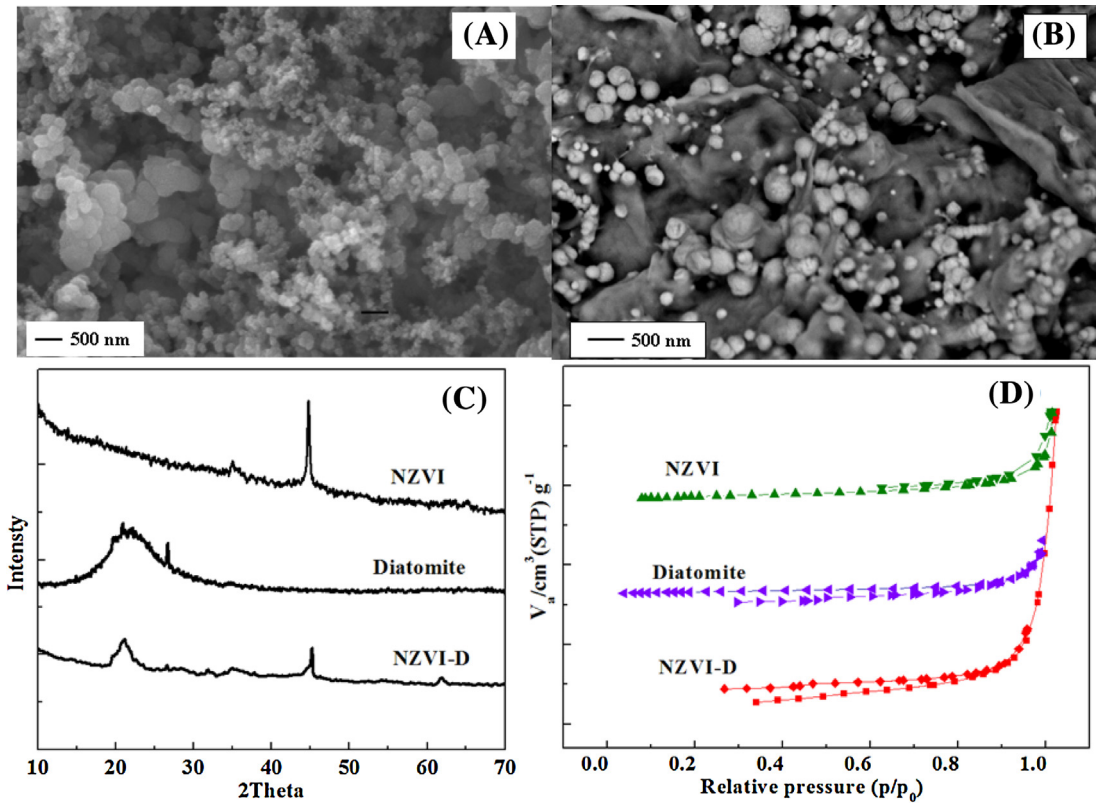

Fig. 1. SEM images of (A) NZVI (B) NZVI-D, (C) XRD patterns, (D) and the N_2 adsorption-desorption isotherms of diatomite, NZVI and NZVI-D samples.

surface with size below the detection limit of XRD [59]. The specific surface areas of diatomite, NZVI and NZVI-D were determined from N_2 adsorption-desorption isotherm analysis. As is shown in Fig. 1D, the three samples exhibit type-IV isotherms, which is characteristic of porous materials. Besides, the presence of a sharp adsorption step in these isotherm curves suggests that the solids possess a well defined array of regular mesopores [59]. Based on these data, the specific surface area (S_{BET}) were determined to be 26.1 m^2/g for diatomite, 42.2 m^2/g for NZVI, 29.5 m^2/g for NZVI-D, respectively.

3.2. Enhanced sequestration of U(VI) by diatomite-supported NZVI

The results for U(VI) sequestration by the reactive materials under different conditions are shown in Fig. 2. Firstly, experiments were conducted to compare the effectiveness of ZVI, NZVI and NZVI-D in U(VI) sequestration with the same initial concentration of 100 mg/L. We can see from Fig. 2A that ~12.2% of U(VI) was sequestered onto diatomite by an adsorption after 90 min. Whereas, ~14.9% of U(VI) was sequestered onto ZVI and ~52.1% of U(VI) was sequestered onto NZVI mainly by a reduction after 90 min, indicating that the sequestration efficiency of NZVI was much higher than that of ZVI. According to the different reactivity of ZVI and NZVI, we can see that the particle size of iron played an important role in U(VI) sequestration. As we know, the particle size of NZVI with a greater specific surface area is smaller than that of ZVI, thus, NZVI can offer more interfaces for U(VI) interaction with iron, accordingly, the performance of U(VI) sequestration onto NZVI was enhanced [62]. More importantly, the NZVI-D exhibited the highest U(VI) sequestration, namely, ~96.8% of U(VI) was sequestered onto NZVI-D after 90 min. In previous investigations, Sheng et al. [8] found that the removal performance of U(VI) in the NZVI treatment system was greatly enhanced using Na-bentonite as a support. Jing et al. [34] reported that illite-supported NZVI displayed a higher removal efficiency of U(VI) from aqueous solution than the bare NZVI did. Besides, Xu et al. [35] reported that the removal of U(VI) on montmorillonite-supported NZVI was much higher than that of the NZVI alone. All these investigations indicated that the removal performance of U(VI) in the supported NZVI treatment system was higher than the sun of NZVI reduction and support adsorption, which is in good agreement with the result observed herein, i.e., the sequestration of U(VI) in the NZVI-D treatment system was higher than the sum of U(VI) adsorption via diatomite and U(VI) reduction via NZVI. This result suggests the good synergistic effect during U(VI) sequestration in the NZVI-D treatment system, which may be related to the high adsorption of U(VI) onto diatomite. We further make a kinetic interpretation about the sequestration of U(VI) onto the reactive materials by a pseudo first-order reaction, which is expressed as, $ln(c/c_0) = -k_{obs} \times t$, whereas, k_{obs} (min^{-1}) is called the observed rate constant of a pseudo first-order reaction. Herein, the plots of $ln(c/c_0)$ versus t produced linear plots with correlation coefficients (R^2) being higher than 0.9, indicating that the rate of U(VI) sequestered onto the reactive materials could be described well by the pseudo first-order model. Besides, the rate constants (k_{obs}) indicative of the reactivity for a given material were fitted to be 0.0008 min^{-1} for diatomite, 0.0011 min^{-1} for ZVI, 0.0052 min^{-1} for NZVI, 0.0213 min^{-1} for NZVI-D, respectively. Namely, the values of k_{obs} were in the following order of NZVI-D > NZVI > ZVI > diatomite, suggesting the well improvements upon the reactivity of NZVI nanoparticles when supported on diatomite.

It was commonly regarded that Fe^0-induced reduction is a surface-mediated reaction, and thus the efficiency of U(VI) sequestration is positively related to U(VI) concentration in the vicinity of iron surface [8,63]. Therefore, a transient U(VI) enrichment step on the solid surface is very necessary for the reduction of dissolved U(VI) by the reactive materials. The adsorption isotherms of U(VI) on diatomite was shown in Fig. S2. The zeta potentials of diatomite at different pH conditions were also determined (Fig. S3). We can

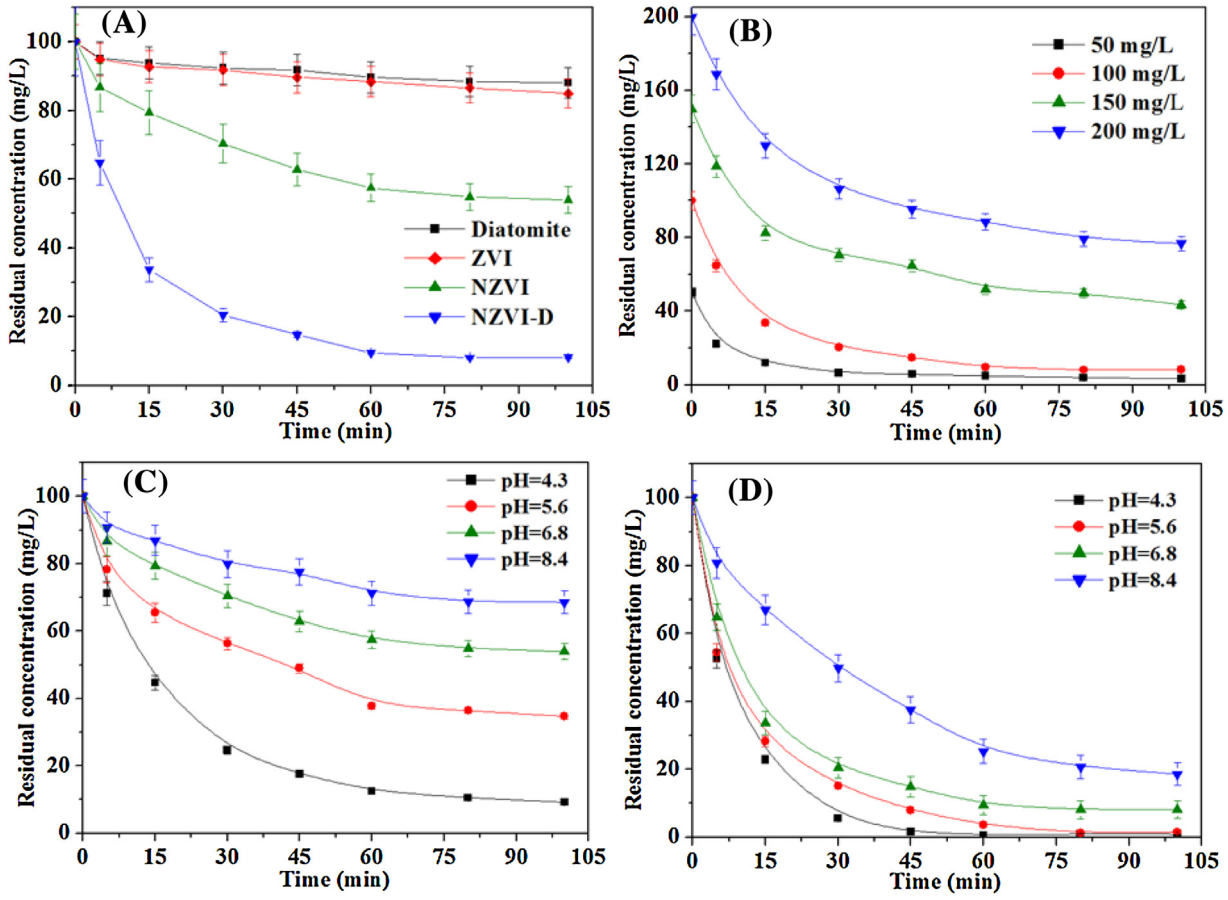

Fig. 2. The comparison of U(VI) sequestered onto various reactive materials (A), the effect of initial concentration on U(VI) sequestered onto NZVI-D (B), and the effect of pH on U(VI) sequestered onto NZVI (C) and NZVI-D (D), respectively.

see that diatomite exhibits negative zeta potentials with pH ranging from 2.0 to 10.0 under the experimental conditions, which is in favor of the adsorption of cationic U(VI) [55–57]. So, lots of U(VI) ions could be enriched onto the negatively-charged diatomite surfaces, resulting in the increased concentration of U(VI) at the reductive surface, which accelerated the reduction of U(VI) in the NZVI-D treatment system.

The effect of initial concentration on U(VI) removal by NZVI-D is shown in Fig. 2B. We can see that U(VI) sequestration decreases with initial concentration increasing. It was reported that U(VI) is a good oxidant and a well-known passivator of Fe^0, as more U(VI) come closely to Fe^0, more Fe^0 can be oxidized and lose their reactivity which results in the decreased sequestration. The reaction products formed on Fe^0 surface will decrease the electron transfer from NZVI to U(VI) and accordingly retard U(VI) reduction [6–9]. Furthermore, for a fixed NZVI-D dose, the total available reactive sites are limited which contributes to a decreased U(VI) sequestration corresponding to an increased initial U(VI) concentration [64].

The effect of pH on U(VI) sequestration on NZVI and NZVI-D are shown in Fig. 2C and D, respectively. The results showed that U(VI) sequestration by NZVI decreased from ~90.8% to ~31.4% after 90 min, with pH increasing from 4.3 to 8.4. It is obvious that pH plays an important role in U(VI) sequestration onto NZVI, namely, a lower pH favored U(VI) sequestration, since corrosion of NZVI was accelerated at lower pH, and consequently the precipitation of reaction products on iron surface was not as favorable, leading to an enhanced sequestration of U(VI) onto NZVI in water [6,25]. Nevertheless, we can see from Fig. 2D that the sequestration of U(VI) by NZVI-D only decreased from ~99.2% to ~82.4% after 90 min, with pH increasing from 4.3 to 8.4, indicating that pH effect on U(VI) sequestration by NZVI-D is less pronounced than that in the NZVI treatment system, which is probably due to the buffering effect of silanol groups on diatomite surfaces. The primary role of silanol groups on diatomite is their ability to generate protons that can maintain medium pH and thus reduce surface passivation of iron. The changes of pH during U(VI) sequestration in both NZVI and NZVI-D treatment systems at initial pH = 6.8 are shown in Fig. S4, and the results suggest that the final pH maintains much lower in the NZVI-D treatment system (~8.0) than that in the NZVI treatment system (~8.6). A similar pH buffering effect was also reported in other minerals (such as kaolinite, bentonite, biotite and quartz) and iron mixed treatment systems [65–67].

The effect of Fe(II) chelating agents (i.e., 1,10-phenanthroline) on the sequestration of U(VI) by NZVI and NZVI-D is shown in Fig. 3A and B, respectively. It is interesting to note that the sequestration of U(VI) in both NZVI and NZVI-D treatment systems was apparently suppressed in the presence of 1,10-phenanthroline under the same conditions, which is due to the formation of stable complex for 1,10-phenanthroline with Fe(II), inhibiting the redox reaction between U(VI) and Fe(II) [25]. This finding confirmed that Fe(II) adsorbed on surfaces was an important reductant for U(VI) sequestration in the iron treatment system, coinciding with the reports by Liang et al. [11–13,68], who found that, in the ZVI treatment system, the adsorbed Fe(II) on the surface of ZVI and freshly-formed iron oxides/hydroxides could effectively reduce Se(IV)/Se(VI) into Se(0)/Se(-II). In a previous report, it was also documented that U(VI) reduction by dissolved Fe(II) does not occur thermodynamically [69]. However, Fe(II) adsorbed on solid surfaces is considered to be a more powerful reductant than dissolved Fe(II). Previously, it was

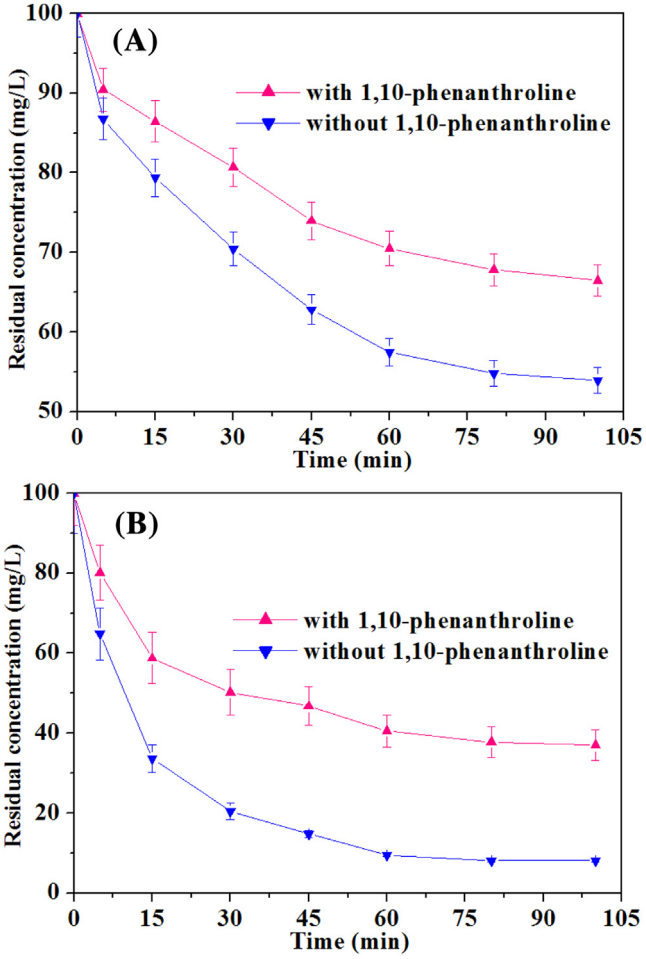

Fig. 3. The suppression of 1,10-phenanthroline on U(VI) sequestered onto (A) NZVI and (B) NZVI-D, respectively.

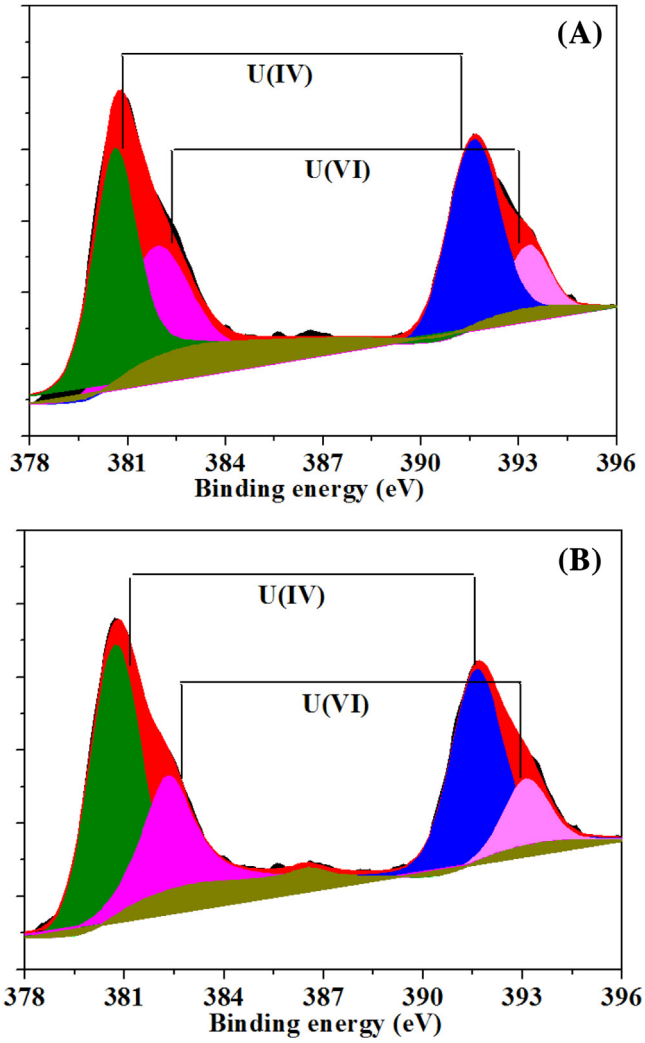

Fig. 4. XPS spectra of curve-fitted U_{4f} photoelectron regions from the NZVI-D samples after reaction with U(VI) for (A) 60 min and (B) 90 min.

indicated that Fe(II) adsorbed on solid surfaces in heterogenous reaction systems could effectively reduce U(VI) to U(IV) [69–72]. In addition, the surface absorbed Fe(II) could increase the conductivity of surface oxidation layer, and lowered the electron transfer barrier over the corrosion coating, thereby significantly enhanced the transfer of electron [12]. So, we believed herein that besides NZVI, Fe(II) adsorbed the freshly-formed iron oxides/hydroxides in the NZVI treatment system also contributed to U(VI) reduction in both NZVI and NZVI-D treatment system. In addition, the effect of 1,10-phenanthroline on U(VI) sequestration is more pronounced in the NZVI-D treatment system than that in the NZVI treatment system, this result indicates that the Fe(II) adsorbed onto diatomite is also able to reduce U(VI) to U(IV).

3.3. Characterization of reaction products by XPS and XAFS

The coordination environment and microstructure of the reaction products can be further determined by XPS and XAFS techniques. The elemental compositions and surface species of the reaction products after reaction were analyzed by XPS. The XPS survey spectra for the NZVI and NZVI-D samples after U(VI) sequestration are shown in Fig. S5. The major identified peaks for both samples were Fe, O, C and U, while only Fe, O and C peaks were identified for pure NZVI sample before reaction (data not shown), which indicated that U(VI) was sequestered on the solid samples. Besides, the intensity of U peak for NZVI-D is much higher than that for NZVI, indicating that more U(VI) can be sequestered on NZVI-D. According to the method in a previous report [73], the relative surface concentrations of U(IV) and U(VI) can be determined from the U_{4f} photoelectron peaks, which can be quantitatively resolved into U(VI) and U(IV) following the binding energies of uranium (Table S1). Since the binding energy of UO_3 (U(VI)) is higher than that of UO_2 (U(IV)), a shift or broadening of the U_{4f} photoelectron peaks to lower energies is indicative of the reduction of U(VI) to a lower oxidation state [73]. Curve fitting for these components was utilized to reveal the relative proportions of U(IV) and U(VI) on the surface of NZVI and NZVI-D. Spectral fitting of the $U_{4f7/2}$ (~380 eV) and $U_{4f5/2}$ (~390 eV) photoelectron peaks from NZVI (Fig. S6) and NZVI-D (Fig. 4) after reaction with U(VI) for 60 min and 90 min revealed that the primary peaks located at 380.5 eV and 391.4 eV, respectively, which is suggestive of U(IV). Whereas, the secondary peaks which is indicative of U(VI) located at 382.3 eV and 393.1 eV, respectively [73]. From the fitting results (data not shown), we can see that the ratios of U(IV) to U(VI) for NZVI, after reaction with U(VI) for 60 and 90 min, were 0.48 and 0.49, respectively, while, the ratios of U(IV) to U(VI) for NZVI-D, after reaction with U(VI) for 60 and 90 min, were 1.97 and 2.01, respectively, This indicated that the reduction of U(VI) into U(IV) by NZVI-D was much higher than that of bare NZVI, namely, the reductive transformation of U(VI) with high toxic and mobility into U(IV) with low toxic and mobility by NZVI could be greatly enhanced using diatomite as a support.

It is well known that XAFS is an element specific, short-range structural probe that provides qualitative and quantitative

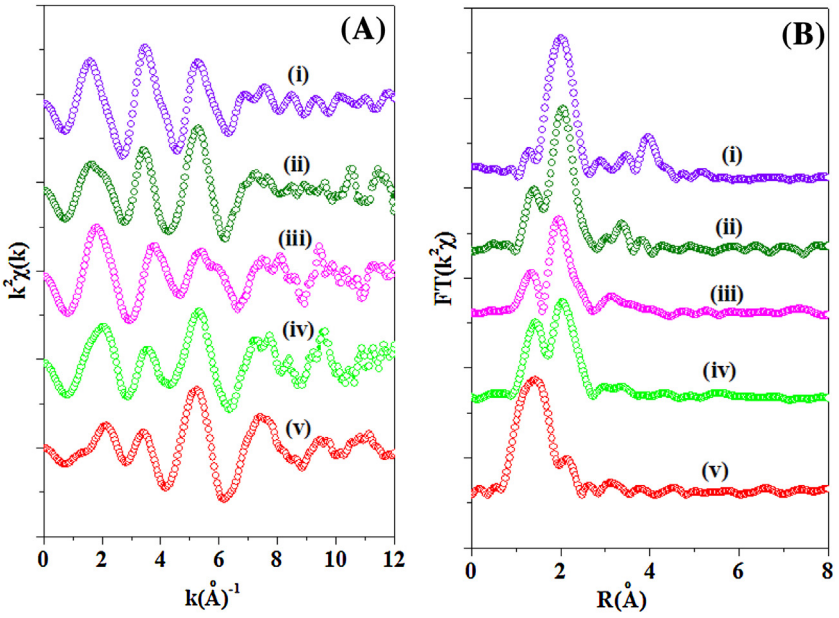

Fig. 5. The U L_{III}-edge background subtracted, k^2-weighted $\chi(k)$ data (A) and corresponding Fourier transformed EXAFS spectra (B) from the reaction samples, U(VI) sequestered onto NZVI-D for (i) 60 min and (ii) 90 min, U(VI) sequestered onto NZVI for (iii) 60 min and (iv) 90 min, and U(VI) adsorbed on diatomite (v).

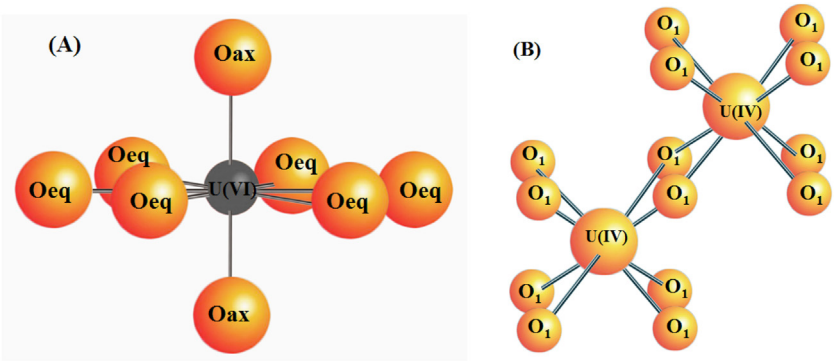

Fig. 6. Ball-and-stick representation of the structure of UO_3 (A) and UO_2 (B).

information on the local structural and compositional environment of the absorbing atom. Herein, data were collected for extended X-ray absorption finem structure (EXAFS), which provides information on the type and number of the atoms surrounding the absorbing atom as well as the radial distances to those atoms [2,4,74–84]. In this way, we can achieve the local atomic environment of U in the samples of U(VI) sequestered onto diatomite, NZVI and NZVI-D via analysis of the EXAFS data. The U L_{III}-edge background subtracted, k^2-weighted $\chi(k)$ data and corresponding Fourier transformed EXAFS spectra of these reaction samples are shown in Fig. 5A and B, respectively. For the sample of U(VI) sequestered onto diatomite, the spectral fits lead to ~2.0 Oax at 1.73 ± 0.02 Å and ~6.0 Oeq at 2.36 ± 0.03 Å, which is a typical structure of uranyl U(VI) (Fig. 6), indicating that U(VI) sequestered onto diatomite is an adsorption procedure without the changes of valence state. Besides, the spectral fits lead to ~1.38 Oax at 1.73 ± 0.02 Å and ~7.6 Oeq/O1 at 2.36 ± 0.03 Å for the sample of U(VI) sequestered onto NZVI, whereas the spectral fits lead to ~0.66 Oax at 1.73 ± 0.03 Å and ~7.9 Oeq/O1 at 2.36 ± 0.05 Å for the sample of U(VI) sequestered onto NZVI-D. The U-Oax shell at ~1.73 Å and the U-Oeq shell at ~2.36 Å indicates the U-O distance of U(VI) (UO_2^{2+}) (Fig. 6A), while the U-O1 shell at ~2.36 Å suggests the U-O distance of U(IV) (UO_2) (Fig. 6B) [4]. It was reported that the coordination number (CN) for the U-O1 shell in a pure UO_2 phase is 8.0 [2]. Nevertheless, the values for the two samples are slightly lower than 8.0 due to the presence of a little amount of UO_2^{2+} with 6 Oeq. Based on the approach proposed in a previous work, the CN value of the U-Oax shell determined from the EXAFS spectrum could be used to estimate the relative amounts of U(IV) and U(VI) in a reaction sample, according to the assumption that U(VI) exists as uranyl ions (UO_2^{2+}) with 2 Oax [4]. Subsequently, we can see from this approach that NZVI contains ~69.0% of U(VI) and ~31.0% of U(IV), while NZVI-D contains ~33.0% of U(VI) and ~67.0% of U(IV), which is in good consistent with the XPS results. Namely, in the NZVI-D treatment system, more U(VI) with high toxic and mobility can be transformed into U(IV) with low toxic and mobility. In addition, for the sample of U(VI) sequestered onto NZVI-D, the spectral fits lead to additional ~1.2 Si at ~3.56 ± 0.04 Å, suggesting that some of the reaction products are well dispersed and in intimate association with the support. Therefore, we can conclude that diatomite could react as a scavenger for the insoluble reaction products and in this way, decrease these insoluble reaction products on NZVI surfaces, which could provide more free area for U(VI) reaction, facilitated NZVI well dispersion and non-agglomeration. This results in a higher reactivity of NZVI which stabilized on diatomite surfaces, thus exhibiting an improved efficiency for U(VI) sequestration [40]. From the analysis of the EXAFS spectroscopic results, we can see that adsorption and reduction occurred concurrently for

U(VI) sequestration in both NZVI and NZVI-D treatment systems. In previous reports [85,86], it was proposed that there are two types of surface sites co-existing on NZVI, i.e., the reactive surface sites and the non-reactive surface sites. In addition, the authors suggested that adsorption reaction takes place on both non-reactive and reactive surface sites, whereas reduction reaction only occurs on the reactive surface sites. According to this model, a conceptual mechanism of U(VI) removal by the iron samples can be further illustrated. Firstly, U(VI) ions in solution attracted to interfaces and formed inner-sphere complexes, which is a relatively fast step. Then, U(VI) ions were reduced into U(IV) mediated by ferrous and/or Fe(0), with the accumulation of reduction products (i.e., UO_2) at interface. At the same time, ferrous and/or Fe(0) were oxidized and precipitated as iron hydroxides, which results in the growing of corrosion products at interface. So, U(VI) can not be completely reduced into U(IV) by NZVI sample, since some of U(VI) could be adsorbed on the corrosion products. Besides, the usage of diatomite as a support could effectively promote the reductive transformation of U(VI) into U(IV) by NZVI sample due to the accumulation of some corrosion products on diatomite surface, which could provide more reactive surface sites for U(VI) reduction. In a word, due to the good advantages of low-cost and environment-friend for zero valent iron [87–90], the diatomite-supported NZVI is a promising material in environmental remediation of U-contaminated wastewater.

4. Conclusions

In conclusions, this study shows that the negatively-charged diatomite is an excellent candidate as a support of NZVI for the sequestration of cationic U(VI) in water. The batch experimental results showed that the sequestration efficiency of U(VI) by diatomite-supported NZVI could be greatly enhanced in comparison with that by bare NZVI, wherein UO_2 were the main reaction products on iron surface. Besides, XPS and XAFS analysis confirmed that the reductive transformation of UO_2^{2+} with high toxic and mobility into UO_2 with low toxic and mobility by diatomite-supported NZVI could be also enhanced, which was due to the synergistic effect between diatomite adsorption and NZVI reduction. The support effect of diatomite in NZVI reaction system strongly depends on its multiple roles including adsorbent of U(VI), pH buffering agent, scavenger for the insoluble reaction products during reaction, and adsorbent of Fe(II) produced in-situ for further reduction of U(VI). The diatomite could also increase the stability and reusability of NZVI during reaction. These results may provide new insights on design and fabrication of supported NZVI environmental remediation of groundwater contaminated with U(VI) and other related radionuclide with the combination of NZVI and natural minerals.

Acknowledgements

Financial supports from the National Natural Science Foundation of China (21577093, 21207092), Natural Science Foundation of Zhejiang Province (LY15B070001) is greatly acknowledged. The authors also thank beamline BL14W1 (Shanghai Synchrotron Radiation Facility) for providing the beam time.

Appendix A. Supplementary data

Supplementary data associated with this article can be found, in the online version, at http://dx.doi.org/10.1016/j.apcatb.2016.04.035.

References

[1] S. Chakraborty, F. Favre, D. Banerjee, A.C. Scheinost, M. Mullet, J.J. Ehrhardt, J. Brendle, L. Vidal, L. Charlet, U(VI) sorption and reduction by Fe(II) sorbed on montmorillonite, Environ. Sci. Technol. 44 (2010) 3779–3785.
[2] E.J. O'Loughlin, S.D. Kelly, R.E. Cook, R. Csencsits, K.M. Kemner, Reduction of uranium(VI) by mixed iron(II)/iron(III) hydroxide (green rust): formation of UO_2 nanoparticles, Environ. Sci. Technol. 37 (2003) 721–727.
[3] L. Sheng, J.B. Fein, Uranium reduction by shewanella oneidensis MR-1 as a function of $NaHCO_3$ concentration: surface complexation control of reduction kinetics, Environ. Sci. Technol. 48 (2014) 3768–3775.
[4] E.J. O'Loughlin, S.D. Kelly, K.M. Kemner, An XAFS investigation of the interactions of U^{VI} with secondary mineralization products from the bioreduction of Fe^{III} oxides, Environ. Sci. Technol. 44 (2010) 1656–1661.
[5] Z. Chen, Z. Zhuang, Q. Cao, X. Pan, X. Guan, Z. Lin, Adsorption-induced crystallization of U-rich nanocrystals on nano-$Mg(OH)_2$ and the aqueous uranyl enrichment, ACS Appl. Mater. Interfaces 6 (2014) 1301–1305.
[6] S. Yan, B. Hua, Z. Bao, C. Liu, B. Deng, Uranium(VI) removal by nanoscale zerovalent iron in anoxic batch systems, Environ. Sci. Technol. 44 (2010) 7783–7789.
[7] C. Ding, W. Cheng, Y. Sun, X. Wang, Effects of Bacillus subtilis on the reduction of U(VI) by nano-Fe^0, Geochim. Cosmochim. Acta 165 (2015) 86–107.
[8] G. Sheng, X. Shao, Y. Li, J. Li, H. Dong, W. Cheng, X. Gao, Y. Huang, Enhanced removal of U(VI) by nanoscale zerovalent iron supported on Na-bentonite and an investigation of mechanism, J. Phys. Chem. A 118 (2014) 2952–2958.
[9] K. Cantrell, D. Kaplan, T. Wietsma, Zero-valent iron for the in situ remediation of selected metals in groundwater, J. Hazard. Mater. 42 (1995) 201–212.
[10] X. Guan, Y. Sun, H. Qin, J. Li, I.M.C. Lo, D. He, H. Dong, The limitations of applying zero-valent iron technology in contaminants sequestration and the corresponding countermeasures: the development in zero-valent iron technology in the last two decades (1994–2014), Water Res. 75 (2015) 224–248.
[11] L. Liang, X. Guan, Z. Shi, J. Li, Y. Wu, P.G. Tratnyek, Coupled effects of aging and weak magnetic fields on sequestration of selenite by zero-valent iron, Environ. Sci. Technol. 48 (2014) 6326–6334.
[12] L. Liang, W. Yang, X. Guan, J. Li, Z. Xu, J. Wu, Y. Huang, X. Zhang, Kinetics and mechanisms of pH-dependent Se(IV) removal by zero valent iron, Water Res. 47 (2013) 5846–5855.
[13] L. Liang, W. Sun, X. Guan, Y. Huang, W. Choi, H. Bao, L. Li, Z. Jiang, Weak magnetic field significantly enhances selenite removal kinetics by zero valent iron, Water Res. 1 (2014) 371–380.
[14] F.G. Simon, C. Segebade, M. Hedrich, Behavior of uranium in iron-bearing permeable reactive barriers: investigation with ^{237}U as a radioindicator, Sci. Total Environ. 307 (2003) 231–238.
[15] J.N. Fiedor, W.D. Bostick, R.J. Jarabek, J. Farrell, Understanding the mechanism of uranium removal from groundwater by zerovalent iron using X-ray photoelectron spectroscopy, Environ. Sci. Technol. 32 (1998) 1466–1473.
[16] S.J. Morrson, D.R. Metzler, C.E. Carpenter, Uranium precipitation in a permeable reactive barrier by progressive irreversible dissolution of zerovalent iron, Environ. Sci. Technol. 35 (2001) 385–390.
[17] B. Gu, L. Liang, M.J. Dickey, X. Yin, S. Dai, Reductive precipitation of uranium(VI) by zerovalent iron, Environ. Sci. Technol. 32 (1998) 3366–3373.
[18] C. Noubactep, A. Schöner, G. Meinrath, Mechanism of uranium removal from the aqueous solution by elemental iron, J. Hazard. Mater. 132 (2006) 202–212.
[19] S.J. Morrison, P.S. Mushovic, P.L. Niesen, Early breakthrough of molybdenum and uranium in a permeable reactive barrier, Environ. Sci. Technol. 40 (2006) 2018–2024.
[20] J. Farrell, W.D. Bostick, R.J. Jarabek, J.N. Fiedor, Uranium removal from ground water using zero valet iron media, Ground Water 37 (1999) 618–624.
[21] Y. Wang, K. Salvage, Immobilization of uranium in the presence of $Fe0_{(s)}$: model development and simulation of contrasting experimental conditions, Appl. Geochem. 20 (2005) 1268–1283.
[22] R.A. Crane, M. Dickinson, I.C. Popescu, T.B. Scott, Magnetite and zero-valent iron nanoparticles for the remediation of uranium contaminated environmental water, Water Res. 45 (2011) 2931–2942.
[23] M. Dickinson, A.B. Scott, The application of zero-valent iron nanoparticles for the remediation uranium-contaminated waste effluent, J. Hazard. Mater. 178 (2010) 171–179.
[24] O. Riba, T.B. Scott, K. Vala Ragnarsdottir, G.C. Allen, Reaction mechanism of uranyl in the presence of zero-valent iron nanoparticles, Geochim. Cosmochim. Acta 72 (2008) 4047–4057.
[25] S. Yan, Y. Chen, W. Xiang, Z. Bao, C. Liu, B. Deng, Uranium(VI) reduction by nanoscale zero-valent iron in anoxic batch systems: the role of Fe(II) and Fe(III), Chemosphere 117 (2014) 625–630.
[26] R.A. Crane, H. Pullin, T.B. Scott, The influence of calcium, sodium and bicarbonate on the uptake of uranium onto nanoscale zero-valent iron particles, Chem. Eng. J. 277 (2015) 252–259.
[27] R.A. Crane, M. Dickinson, T.B. Scott, Nanoscale zero-valent iron particles for the remediation of plutonium and uranium contaminated solutions, Chem. Eng. J. 262 (2015) 319–325.
[28] I.C. Popescu, P. Filip, D. Humelnicu, I. Humelnicu, T.B. Scott, R.A. Crane, Removal of uranium(VI) from aqueous systems by nanoscale zero-valent iron particles suspended in carboxy-methyl cellulose, J. Nucl. Mater. 443 (2013) 250–255.

[29] T.B. Scott, I.C. Popescu, R.A. Crane, C. Noubactep, Nano-scale metallic iron for the treatment of solutions containing multiple inorganic contaminants, J. Hazard. Mater. 186 (2011) 280–287.
[30] C. Gu, H.Z. Jia, H. Li, J.B. Teppen, A.S. Boyd, Synthesis of highly reactive subnanosized zero-valent iron using smectite clay templates, Environ. Sci. Technol. 44 (2010) 4258–4263.
[31] O. Celebi, C. Üzüm, T. Shahwan, H.N. Erten, A radiotracer study of the adsorption behavior of aqueous Ba^{2+} ions on nanoparticles of zero-valent iron, J. Hazard. Mater. 148 (2007) 761–767.
[32] T. Phenrat, N. Saleh, K. Sirk, R.D. Tilton, G.V. Lowry, Aggregation and sedimentation of aqueous nanoscale zerovalent iron dispersions, Environ. Sci. Technol. 41 (2007) 284–290.
[33] Z. Liu, C. Gu, M. Ye, Y. Bian, Y. Cheng, F. Wang, X. Yang, Y. Song, X. Jiang, Debromination of polybrominated diphenyl ethers by attapulgite-supported Fe/Ni bimetallic nanoparticles: influencing factors, kinetics and mechanism, J. Hazard. Mater. 298 (2015) 328–337.
[34] C. Jing, Y. Li, R. Cui, J. Xu, Illite-supported nanoscale zero-valent iron for removal of ^{238}U from aqueous solution: characterization, reactivity and mechanism, J. Radioanal. Nucl. Chem. 304 (2015) 859–865.
[35] J. Xu, Y. Li, C. Jing, H. Zhang, Y. Ning, Removal of uranium from aqueous solution using montmorillonite-supported nanoscale zero-valent iron, J. Radioanal. Nucl. Chem. 299 (2014) 329–336.
[36] S. Luo, P. Qin, J. Shao, L. Peng, Q. Zeng, J.D. Gu, Synthesis of reactive nanoscalezero valent iron using rectorite supports and its application for orange II removal, Chem. Eng. J. 223 (2013) 1–7.
[37] L. Shi, X. Zhang, Z. Chen, Removal of chromium(VI) from wastewater using bentonite-supported nanoscale zero-valent iron, Water Res. 45 (2011) 886–892.
[38] L. Shi, Y. Lin, X. Zhang, Z. Chen, Synthesis, characterization and kinetics of bentonite supported nZVI for the removal of Cr(VI) from aqueous solution, Chem. Eng. J. 171 (2011) 612–617.
[39] X. Sun, Y. Yan, J. Li, W. Han, L. Wang, SBA-15-incorporated nanoscale zero-valent iron particles for chromium(VI) removal from groundwater: mechanism, effect of pH, humic acid and sustained reactivity, J. Hazard. Mater. 266 (2014) 26–33.
[40] E. Petala, K. Dimos, A. Douvalis, T. Bakas, J. Tucek, R. Zboril, M. Karakassides, Nanoscale zero-valent iron supported on mesoporous silica: characterization and reactivity for Cr(VI) removal from aqueous solution, J. Hazard. Mater. 261 (2013) 295–306.
[41] R. Saad, S. Thiboutot, G. Ampleman, W. Dashan, J. Hawari, Degradation of trinitroglycerin (TNG) using zero-valent iron nanoparticles/nano silica SBA-15 composite (ZVINs/SBA-15), Chemosphere 81 (2010) 853–858.
[42] J. Zhan, T. Zheng, G. Piringer, C. Day, G.L. McPerson, Y. Lu, K. Papadopoulos, V.T. John, Transport characteristics of nanoscale functional zerovalent iron/silica composites for in situ remediation of trichloroethylene, Environ. Sci. Technol. 42 (2008) 8871–8876.
[43] Z. Jiang, L. Lv, W. Zhang, Q. Du, B. Pan, L. Yang, Q. Zhang, Nitrate reduction using nanosized zero-valent iron supported by polystyrene resins: role of surface functional groups, Water Res. 45 (2011) 2191–2198.
[44] A. Li, C. Tai, Z. Zhao, Y. Wang, Q. Zhang, G. Jiang, J. Hu, Debromination of decabrominated diphenyl ether by resin-bound iron nanoparticles, Environ. Sci. Technol. 41 (2007) 6841–6846.
[45] M. Liu, Y. Wang, L. Chen, Y. Zhang, Z. Lin, $Mg(OH)_2$ supported nanoscale zero valent iron enhancing the removal of Pb(II) from aqueous solution, ACS Appl. Mater. Interfaces 7 (2015) 7961–7969.
[46] X. Lv, J. Xu, G. Jiang, X. Xu, Removal of chromium(VI) from wastewater by nanoscale zero-valent iron particles supported on multiwalled carbon nanotubes, Chemosphere 85 (2011) 1204–1209.
[47] T. Zheng, J. Zhan, J. He, C. Day, Y. Lu, G.L. McPerson, G. Piringer, V.T. John, Reactivity characteristics of nanoscale zerovalent iron-silica composites for trichloroethylene remediation, Environ. Sci. Technol. 42 (2008) 4494–4499.
[48] R.A. Crane, T.B. Scott, The removal of uranium onto carbon-supported nanoscale zero-valent iron particles, J. Nano Res. 16 (2015) 1–13.
[49] M. Xing, L. Xu, J. Wang, Mechanism of Co(II) adsorption by zero valent iron/grapheme nanocomposite, J. Hazard. Mater. 301 (2016) 286–296.
[50] J. Li, C. Chen, R. Zhang, X. Wang, Nanoscale zero-valent iron particles supported on reduced graphene oxides by using a plasma technique and their application for removal of heavy-metal ions, Chem. Asian J. 10 (2015) 1410–1417.
[51] Y. Sun, C. Ding, W. Cheng, X. Wang, Simultaneous adsorption and reduction of U(VI) on reduced graphene oxide-supported nanoscale zerovalent iron, J. Hazard. Mater. 280 (2014) 399–408.
[52] Z. Li, L. Wang, L. Yuan, C. Xiao, L. Mei, L. Zheng, J. Zhang, J. Yang, Y. Zhao, Z. Zhu, Z. Chai, W. Shi, Efficient removal of uranium from aqueous solution by zero-valent iron nanoparticle and its graphene composite, J. Hazard. Mater. 290 (2015) 26–33.
[53] G. Sheng, A. Alsaedi, W. Shammakh, S. Monaquel, J. Sheng, X. Wang, H. Li, Y. Huang, Enhanced sequestration of selenite in water by nanoscale zero valent iron immobilization on carbon nanotubes by a combined batch, XPS and XAFS investigation, Carbon 99 (2016) 123–130.
[54] G. Sheng, J. Hu, X. Wang, Sorption properties of Th(IV) on the raw diatomite-effects of contact time pH, ionic strength and temperature, Appl. Radiat. Isot. 66 (2008) 1313–1320.
[55] G. Sheng, S. Wang, J. Hu, Y. Lu, J. Li, Y. Dong, X. Wang, Adsorption of Pb(II) on diatomite as affected via aqueous solution chemistry and temperature, Colloids Surf. A 339 (2009) 159–166.
[56] G. Sheng, S. Yang, J. Sheng, J. Hu, X. Tan, X. Wang, Macroscopic and microscopic investigation of Ni(II) sequestration on diatomite by batch, XPS and EXAFS techniques, Environ. Sci. Technol. 45 (2011) 7718–7726.
[57] G. Sheng, H. Dong, Y. Li, Characterization of diatomite and its application for the retention of radiocobalt: role of environmental parameters, J. Environ. Radioac. 113 (2012) 108–115.
[58] G. Sheng, R. Shen, H. Dong, Y. Li, Colloidal diatomite, radionickel and humic substance interaction: a combined batch, XPS and EXAFS investigation, Environ. Sci. Pollut. Res. 20 (2013) 3708–3717.
[59] Z. Sun, S. Zheng, G.A. Ayoko, R.L. Frost, Y. Xi, Degradation of simazine from aqueous solutions by diatomite-supported nanosized zero-valent iron composite materials, J. Hazard. Mater. 263 (2013) 768–777.
[60] I. Dror, O. Jacov, A. Cortis, B. Berkowitz, Catalytic transformation of persistent contaminants using a new composite material based on nanosized zero-valent iron, ACS Appl. Mater. Interfaces 4 (2012) 3416–3423.
[61] Y. Li, W. Cheng, G. Sheng, J. Li, H. Dong, Y. Chen, L. Zhu, Synergetic effect of a pillared bentonite support on Se(VI) removal by nanoscale zero valent iron, Appl. Catal. B: Environ. 174–175 (2015) 329–335.
[62] G.V. Lowry, K.M. Johnson, Congener-specific dechlorination of dissolved PCBs by microscale and nanoscale zerovalent iron in a water/methanol solution, Environ. Sci. Technol. 38 (2004) 5208–5216.
[63] D. Zhao, X. Wang, S. Yang, Z. Guo, G. Sheng, Impact of water quality parameters on the sorption of U(VI) onto hematite, J. Environ. Radioact. 103 (2012) 20–29.
[64] T. Liu, L. Zhao, D. Sun, X. Tan, Entrapment of nanoscale zero-valent iron in chitosan beads for hexavalent chromium removal from wastewater, J. Hazard. Mater. 184 (2010) 724–730.
[65] D.W. Cho, C.M. Chon, B.H. Jeon, Y. Kim, M.A. Khan, H. Song, The role of clay minerals in the reduction of nitrate in groundwater by zero-valent iron, Chemosphere 81 (2010) 611–616.
[66] R.M. Powell, R.W. Puls, Proton generation by dissolution of intrinsic or augmented aluminosilicate minerals for in situ contaminant remediation by zero-valence-state iron, Environ. Sci. Technol. 31 (1997) 2244–2251.
[67] D.W. Blowes, C.J. Ptacek, J.L. Jambor, In-situ remediation of Cr(VI)-contaminated groundwater using permeable reactive walls: laboratory studies, Environ. Sci. Technol. 31 (1997) 3348–3357.
[68] L. Liang, X. Guan, Y. Huang, J. Ma, X. Sun, J. Qiao, G. Zhou, Efficient selenate removal by zero-valent iron in the presence of weak magnetic field, Sep. Purif. Technol. 156 (2015) 1064–1072.
[69] E. Liger, L. Charlet, P. Van Cappellen, Surface catalysis of uranium(VI) reduction by iron(II), Geochim. Cosmochim. Acta 63 (1999) 2939–2955.
[70] J.H. Jang, B.A. Dempsey, W.D. Burgos, Reduction of U(VI) by Fe(II) in the presence of hydrous ferric oxide and hematite: effects of solid transformation, surface coverage, and humic acid, Water Res. 42 (2008) 2269–2277.
[71] B.H. Jeon, B.A. Dempsey, W.D. Burgos, M.O. Barnett, E.E. Roden, Chemical reduction of U(VI) by Fe(II) at the solid-water interface using natural and synthetic Fe(III) oxides, Environ. Sci. Technol. 39 (2005) 5642–5649.
[72] P.M. Fox, J.A. Davis, R. Kukkadapu, D.M. Singer, J. Bargar, K.H. Williams, Abiotic U(VI) reduction by sorbed Fe(II) on natural sediments, Geochim. Cosmochim. Acta 17 (2013) 266–282.
[73] T.B. Scott, G.C. Allen, P.J. Heard, M.G. Randell, Reduction of U(VI) to U(IV) on the surface of magnetite, Geochim. Cosmochim. Acta 69 (2005) 5639–5646.
[74] G. Sheng, S. Yang, Y. Li, X. Gao, Y. Huang, X. Wang, Retention mechanisms and microstructure of Eu(III) on manganese dioxide studied by batch and high resolution EXAFS technique, Radiochim. Acta 102 (2014) 155–167.
[75] G. Sheng, L. Ye, Y. Li, H. Dong, H. Li, X. Gao, Y. Huang, EXAFS study of the interfacial interaction of nickel(II) on titanate nanotubes: role of contact time, pH and humic substances, Chem. Eng. J. 248 (2014) 71–78.
[76] G. Sheng, S. Yang, D. Zhao, J. Sheng, X. Wang, Adsorption of Eu(III) on titanate nanotubes studied by a combination of batch and EXAFS technique, Sci. China: Chem. 55 (2012) 182–194.
[77] G. Sheng, H. Dong, R. Shen, Y. Li, Microscopic insights into the temperature-dependent adsorption of Eu(III) onto titanate nanotubes studied by FTIR, XPS XAFS and batch technique, Chem. Eng. J. 217 (2013) 486–494.
[78] Y. Sun, X. Guan, J. Wang, X. Meng, C. Xu, G. Zhou, Effect of weak magnetic field on arsenate and arsenite removal from water by zerovalent iron: an XAFS investigation, Environ. Sci. Technol. 48 (2014) 6850–6858.
[79] J. Li, Z. Shi, B. Ma, P. Zhang, X. Jiang, Z. Xiao, X. Guan, Improving the reactivity of zerovalent iron by taking advantage of its magnetic memory: implications for arsenite removal, Environ. Sci. Technol. 49 (2015) 10581–10588.
[80] G. Sheng, Q. Yang, F. Peng, H. Li, X. Gao, Y. Huang, Determination of colloidal pyrolusite, Eu(III) and humic substance interaction: a combined batch and EXAFS approach, Chem. Eng. J. 245 (2014) 10–16.
[81] M.J. Wharton, B. Atkins, J.M. Charnock, F.R. Livens, R.A.D. Pattrick, D. Collison, An X-ray absorption spectroscopy study of the coprecipitation of Tc and Re with mackinawite (FeS), Appl. Geochem. 15 (2000) 347–354.
[82] G. Sheng, J. Hu, H. Li, J. Li, Y. Huang, Enhanced sequestration of Cr(VI) by nanoscale zero-valent iron supported on layered double hydroxide by batch and XAFS study, Chemosphere 148 (2016) 227–232.
[83] X. Gao, G. Sheng, Y. Huang, Mechanism and microstructure of Eu(III) interaction with γ-MnOOH by a combination of batch and high resolution EXAFS investigation, Sci. China: Chem. 56 (2013) 1658–1666.
[84] X. Gao, S. Gu, Q. Gao, Y. Zou, Z. Jiang, S. Zhang, X. Wei, H. Yu, G. Sheng, P. Duan, Y. Huang, A high-resolution X-ray fluorescence spectrometer and its application at SSRF, X-ray Spectrom. 42 (2013) 502–507.

[85] R. Cheng, J. Wang, W. Zhang, Comparison of reductive dechlorination of p-chlorophenol using Fe^0 and nanosized Fe^0, J. Hazard. Mater. 144 (2007) 334–339.
[86] B.L. Deng, S.D. Hu, T.M. Whitworth, R. Lee, Chlorinated Solvent and Dnapl Remediation ACS Symposium Series, vol. 837, Trichloroethylene Reduction on Zero-Valent Iron: Probing Reactive versus Nonreactive Sites (2003) 181–205.
[87] C. Tang, Y.H. Huang, H. Zeng, Z. Zhang, Reductive removal of selenate by zero-valent iron: the roles of aqueous Fe^{2+} and corrosion products, and selenate removal mechanisms, Water Res. 67 (2014) 166–274.
[88] J. Li, H. Qin, X. Guan, Premagnetization for enhancing the reactivity of multiple zerovalent iron samples toward various contaminants, Environ. Sci. Technol. 49 (2015) 14401–14408.
[89] Y.H. Huang, C. Tang, H. Zeng, Removing molybdate from water using a hybridized zero-valent iron/magnetite/Fe(II) treatment system, Chem. Eng. J. 200–202 (2012) 257–263.
[90] C. Tang, Y. Huang, Z. Zhang, J. Chen, H. Zeng, Y.H. Huang, Rapid removal of selenate in a zero-valent iron/Fe_3O_4/Fe^{2+} synergetic system, Appl. Catal. B: Environ. 184 (2016) 320–327.